Complete and incomplete fusion of 6 MeV/nucleon light heavy ions on ^{51}V

D. J. Parker
Nuclear Physics and Instrumentation Division, Harwell Laboratory, Oxfordshire, OX11 0RA, United Kingdom

J. J. Hogan
Department of Chemistry, McGill University, Montreal, Quebec, Canada H3A 2K6

J. Asher
Nuclear Physics and Instrumentation Division, Harwell Laboratory, Oxfordshire, OX11 0RA, United Kingdom
(Received 20 September 1988)

The reactions of 6 MeV/nucleon ^{12}C, ^{15}N, ^{16}O, ^{19}F, and ^{20}Ne ions on ^{51}V have been studied by measuring the yields and projected recoil range distributions of radioactive reaction residues and the inclusive spectra of emitted projectile-like fragments. Modelling of the reaction mechanism in terms of contributions from complete fusion and various incomplete fusion processes, on the hypothesis that the observed projectile-like fragments are essentially all due to incomplete fusion, leads to good agreement with the observed yields and recoil distributions. The results are discussed in the context of the sum rule model of incomplete fusion.

I. INTRODUCTION

Above the Coulomb barrier, the reaction cross section in reactions of light heavy ions is dominated by the mechanism of fusion/evaporation. However, it has long been realised that, in addition to complete fusion, various incomplete fusion processes may contribute significantly to the yields of evaporation residues. Any attempt to develop a model for calculating reaction yields should take account of these incomplete fusion processes.

In the years since Inamura *et al.*[1] first identified incomplete fusion as a mechanism, considerable work has been done in clarifying the microscopic nature of the process.[2] It is now generally accepted that the various incomplete fusion processes occur for incident partial waves generally higher than those involved in complete fusion, but that the windows in l space associated with the different processes overlap to a considerable extent. Most studies have been carried out by particle-γ coincidence measurements; these enable the detailed mechanism of a particular process to be established, but may be less useful in determining absolute cross sections.

In contrast, we have been using radioactive recoil studies to investigate the cross sections for forming reaction residues by complete and incomplete fusion.[3,4] For a radioactive reaction residue, we measure the yield and also the differential recoil range distribution; in principle this enables us to determine the absolute contribution to the yield of each residue from each of the processes present. Each fusion process forms an excited intermediate, whose recoil velocity is approximately proportional to the mass of the fusing particle, so that different fusion processes form residues with different characteristic recoil velocities.

In our original study of $^{12}C+^{51}V$ (Ref. 3), the contributions of the two strong incomplete fusion processes, involving escape of one and two α particles, respectively, and of complete fusion could be clearly distinguished in the recoil distributions for the various residues; from these the total cross section for each of the two incomplete fusion processes was deduced. Over a range of incident energies from just above the Coulomb barrier up to 100 MeV, it was found that the deduced incomplete fusion processes accounted for all the observed fast α particles in the measured inclusive spectra.

A subsequent study of $^{20}Ne+^{93}Nb$ (Ref. 4) showed breakup of the ^{20}Ne projectile in a number of different ways and a variety of different incomplete fusion processes in the measured recoil distributions. It was not possible to separate these processes unambiguously by analysis of the recoil distributions alone; instead we adopted the hypothesis that essentially all of the projectile-like fragments observed in the measured inclusive particle spectra are spectator fragments accompanying incomplete fusion, and calculated the cross sections and recoil distributions expected on this basis, using the statistical-mode code CASCADE (Ref. 5). The results were reasonably consistent with the measured data, suggesting that this hypothesis is realistic.

The present paper reports further studies of reactions on ^{51}V using these techniques. To supplement the reactions of ^{12}C previously studied, we have used the projectiles ^{16}O, ^{20}Ne, ^{15}N, and ^{19}F. The first two of these may be considered α particle composites, like ^{12}C, while the last two presumably have a more complex cluster structure. Reactions of these projectiles were all studied at the same velocity (an incident energy of 6 MeV/nucleon).

II. EXPERIMENTAL METHOD

Beams of 96 MeV ^{16}O, 120 MeV ^{20}Ne, 90 MeV ^{15}N, and 115 MeV ^{19}F from the Harwell Variable Energy Cyclotron were each used for three separate measurements on vanadium targets, measuring, respectively, the emitted particle spectra, the cross sections for forming various radioactive residues, and the differential recoil range distri-

butions for these residues. The techniques used were similar to those reported previously,[3,4] and are briefly summarised following.

A. Particle spectra

The energy spectra of emitted alpha particles, boron, carbon, nitrogen, oxygen, and fluorine were measured at a number of laboratory angles between 10° and 150° using a $\Delta E/E$ telescope of silicon surface-barrier detectors. A rolled vanadium target of thickness approximately 1 mg/cm^2 was mounted normal to the beam axis, except during measurement of spectra close to 90° for which the target angle was displaced by 15°. The target thickness in each run was determined by weighing, to an accuracy of 10%. The targets were nominally 99.99% vanadium, but contained light impurities (principally hydrogen and oxygen) at levels approaching 1 at.%.

An E detector, 3 mm thick, was used with a 15-μm-thick ΔE detector, except for the portion of the α-particle spectra above 20 MeV which was measured using a 50-μm-thick ΔE detector. In many of the runs, a more complicated telescope consisting of two ΔE detectors (15 μm and 10 μm, respectively) was used; the second ΔE detector assisted in discriminating against elastically scattered beam detected at forward angles. The signals from the detectors were digitised and stored event-by-event using a PDP 11/34 computer. Subsequently the data were sorted into maps of total energy $E+\Delta E$ vs a characteristic particle identifier, and the total energy spectrum for each particle type was extracted. No significant yields of ^{3}He or of lithium or beryllium isotopes were detected; for elements above $Z=4$ the resolution of these measurements was insufficient to resolve contributions from different isotopes of the same element.

The measured spectra have been normalised so as to give the double-differential cross section $d^2\sigma/dE\,d\Omega$, in mb/(MeV sr), using the total beam fluence (measured in an electrically suppressed Faraday cup mounted behind the target), the measured target thickness, and the known detector solid angle (0.38 msr). The absolute normalisation is thus believed to be accurate to within 10%, but the relative normalisation of the various spectra within a given run should be consistent to better than 5%. As an example of the data, Figs. 1 and 2 show the spectra obtained with the ^{16}O projectile; the spectra obtained with the other projectiles are qualitatively similar, although the number of species detected increases with the Z of the projectile.

B. Residue cross sections

The absolute cross sections for producing various radioactive residues were measured by irradiating a thin vanadium target, backed by a thick aluminium catcher, and using off-line γ-ray spectrometry to determine residue yields. For each irradiation, the target consisted of approximately 400 μg/cm^2 of vanadium, evaporated onto a support of 200 μg/cm^2 Al; the target was mounted inside the Faraday cup with the V layer upstream, and a further three aluminium foils, each 3 mg/cm^2 thick, were mounted immediately behind the target so as to catch all of the products recoiling out of the target.

Following irradiation [approximately 20-particle nA (pnA) for 4 h], the target and catchers were counted together at a distance of 100 mm from a 15%-efficient Ge(Li) detector. A continuous sequence of counts was performed, starting 20 min after the end of irradiation and continuing for several days. Absolute activities of the radionuclides present were extracted from the γ-ray spectra, using the computer code GAMANAL (Ref 6) and the measured efficiency of the detector in this geometry (known to within 5%). Decay curve analysis was then used to extract the initial activity value for each product.

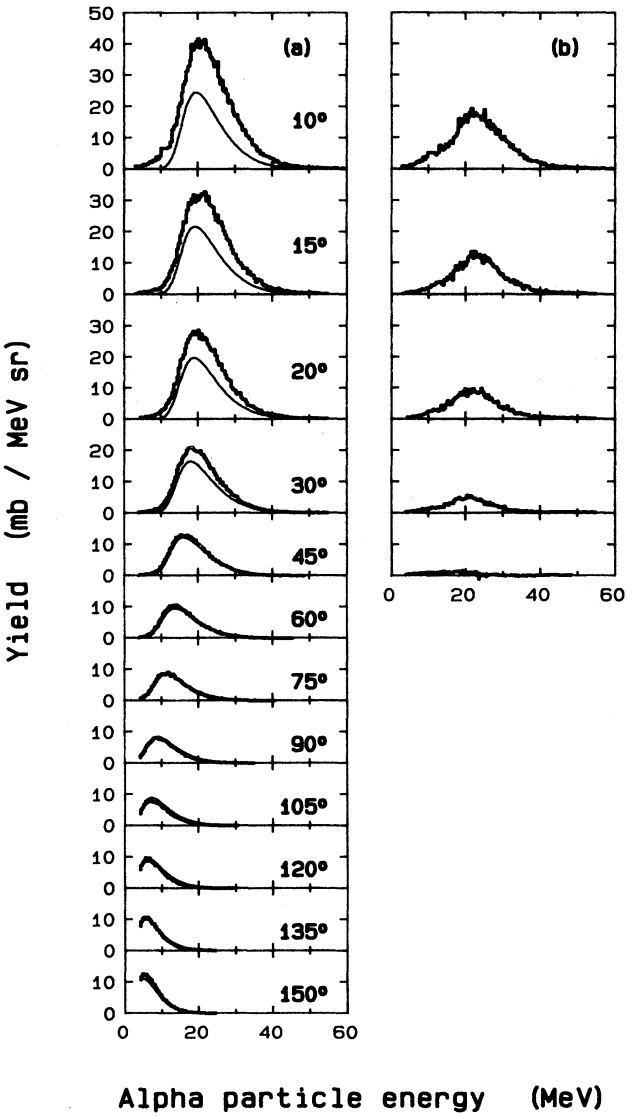

FIG. 1. (a) Measured α-particle spectra from reactions of 96 MeV ^{16}O on ^{51}V. The smooth curves show the calculated evaporative component, fitted to the data at backward angles. (b) The fragment component of the α-particle spectra, obtained by subtracting the curves in Fig. 1(a) from the data.

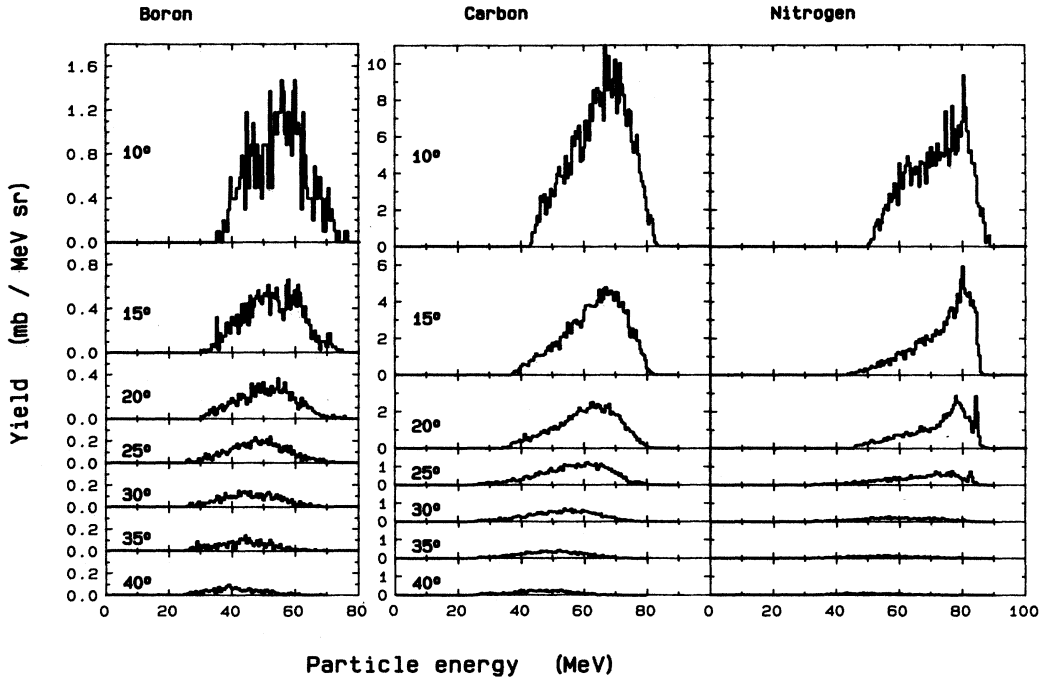

FIG. 2. Measured spectra of boron, carbon, and nitrogen fragments from the reactions of 96 MeV ^{16}O on ^{51}V.

The products studied are listed in Table I with the γ rays used; the branching ratios and half-lives were taken from the GSI Gamma Catalog.[7]

Some weeks after the original irradiation, the thickness of the vanadium layer on each target used was determined by means of activation analysis, using a 9.15-MeV proton beam from the Harwell Tandem Accelerator to generate ^{51}Cr. The amount of ^{51}Cr produced in each target was measured by γ-ray spectrometry, and the known cross section for the $^{51}V(p,n)^{51}Cr$ reaction[8] was used to establish the thickness of vanadium present.

TABLE I. Product residues studied, with γ rays used in their determination. CUM indicates that the yield includes any yield of β-decay precursors formed; in most cases the yield of precursors is predicted to be very small, but has been included in the modelling.

Nuclide	Half-life	E_γ (keV)	Branching ratio (%)	Mode
^{66}Ga	9.3 h	1039	38.4	CUM
^{65}Zn	244 d	1115	50.7	CUM
^{63}Zn	38.4 min	670	8.4	CUM
^{62}Zn	9.13 h	597	26.0	CUM
^{61}Cu	3.41 h	283	13.1	CUM
^{60}Cu	23.2 min	1333	88.0	CUM
^{58}Co	70.8 d	811	99.4	IND
^{57}Co	270.9 d	122	85.6	IND
^{56}Co	78.8 d	847	99.9	IND
^{56}Mn	2.58 h	847	98.9	CUM
^{54}Mn	312.5 d	835	100.0	IND

For each of the four original irradiations, this target thickness was then used, together with the measured beam fluence, to convert the measured activity values for the residues into production cross sections. The results obtained are listed in Table II. The principal uncertainty arises from the uncertainty in normalisation, due to uncertainties in target thickness and fluence measurement, and is estimated at 10%

C. Recoil range distributions

The projected recoil range distributions for the radioactive residues listed in Table I were measured by irradiating a thin vanadium target backed by a stack of thin aluminium catcher foils, and using off-line γ-ray spectrometry to determine the distribution of each residue through the catcher stack. For each irradiation the target consisted of approximately 100 $\mu g/cm^2$ V evaporated onto a support of 200 $\mu g/cm^2$ Al; this target was mounted inside the Faraday cup with the vanadium layer downstream followed immediately by a stack of 25 thin evaporated Al catcher foils, each of thickness between 100 and 200 $\mu g/cm^2$. The thickness of each catcher foil had been determined prior to use, to an uncertainty of approximately 5%, by measuring the energy lost by 5.8 MeV α particles from a ^{244}Cm source in traversing the foil.

Following each irradiation, the catcher foils were counted in turn against the face of a 25%-efficient Ge(Li) detector, at intervals over a period from about 20 min after irradiation up to several weeks later. The activities of the nuclides listed in Table I and present in each catch-

er were extracted from the γ-ray spectra, as described in the preceding section, and the distribution of each residue as a function of depth in the catcher stack was obtained by dividing the measured activity in each catcher by the measured catcher thickness. The normalisation of each distribution was taken from the corresponding cross-section measurement, obtained as described in the preceding section.

The recoil range distributions obtained using the four different projectiles for products from ^{54}Mn up are shown in Figs. 3–6. No recoil distributions are reported for products lighter than ^{54}Mn, because the data were found to be contaminated due to activation of ^{39}K, which was present in small quantities in the catcher foils (probably

TABLE II. Yields of radioactive product residues from the four entrance channels (mb).

				^{15}N+^{51}V					
	^{62}Zn	^{61}Cu	^{60}Cu	^{58}Co	^{57}Co	^{56}Mn	^{54}Mn		
Measured	2.6	72	6.8	232	46	12.9	31.8		
Modelled									
C.F.	1.6	71	11.8	184	61	32	9.4		
(^{15}N, α)				15	2.4	4.1	1.5		
(^{15}N,^{8}Be)						3.4	2.0		
(^{15}N,^{11}B)							5.5		
Totals	1.6	71	11.8	199	63	39.5	18.4		
Without ^{8}Be	1.6	71	11.8	214	66	40.2	17.9		
				^{16}O+^{51}V					
	^{63}Zn	^{62}Zn	^{61}Cu	^{60}Cu	^{58}Co	^{57}Co	^{56}Co	^{56}Mn	^{54}Mn
Measured	24	13	36	14	73	77	21	2.0	75
Modelled									
C.F.	14	20	33	12.2	64	107	27	4.0	48
(^{16}O,α)			0.2	0.7	2	12	3.6	0.5	5.9
(^{16}O,^{8}Be)					3	7.6	1.7	0.5	4.6
(^{16}O,^{11}B)									3.6
(^{16}O,^{12}C)									20
Totals	14	20	33	12.9	69	127	32	5.0	82
Without ^{8}Be	14	20	33	13.6	68	131	34	5.0	84
				^{19}F+^{51}V					
	^{65}Zn	^{63}Zn	^{62}Zn	^{61}Cu	^{60}Cu	^{58}Co	^{57}Co	^{56}Mn	^{54}Mn
Measured	78	26	7.5	58	1.9	87	12	4.8	33.5
Modelled									
C.F.	43	14	7.1	92	4.9	94	14.2	12.0	0.5
(^{19}F,α)		0.4	0.4	4.2	0	17	2.1	3.0	0.4
(^{19}F,^{8}Be)						5	1.4	1.8	1.6
(^{19}F,^{11}B)						0.2	0.9	0.2	0.9
(^{19}F,^{12}C)								1.9	8.6
(^{19}F,^{15}N)									6.9
Totals	66	14.4	7.5	96	4.9	116	18.6	18.9	18.9
Without ^{8}Be	66	14.8	7.9	100	4.9	128	19.3	20.1	17.7
				^{20}Ne+^{51}V					
	^{66}Ga	^{65}Zn	^{63}Zn	^{62}Zn	^{61}Cu	^{58}Co	^{57}Co	^{54}Mn	
Measured	39	88	64	11.6	40	47	44	56	
Modelled									
C.F.	35	80	62	19	40	54	73	12.1	
(^{20}Ne,α)			3.8	0.1	5.9	10.7	29	5.9	
(^{20}Ne,^{8}Be)					4.0	10.0	14.8	4.3	
(^{20}Ne,^{12}C)						1.6	6	5.0	
(^{20}Ne,^{15}N)								11.8	
(^{20}Ne,^{16}O)								36	
Totals	35	80	66	19	50	76	123	75	
Without ^{8}Be	35	80	70	19	52	77	137	77	

as a surface contaminant originating in the detergent used to release the foils during manufacture)—this manifests itself as a level of activity which continues to the back of the catcher stack, rather than showing some maximum range as all products from the target must.

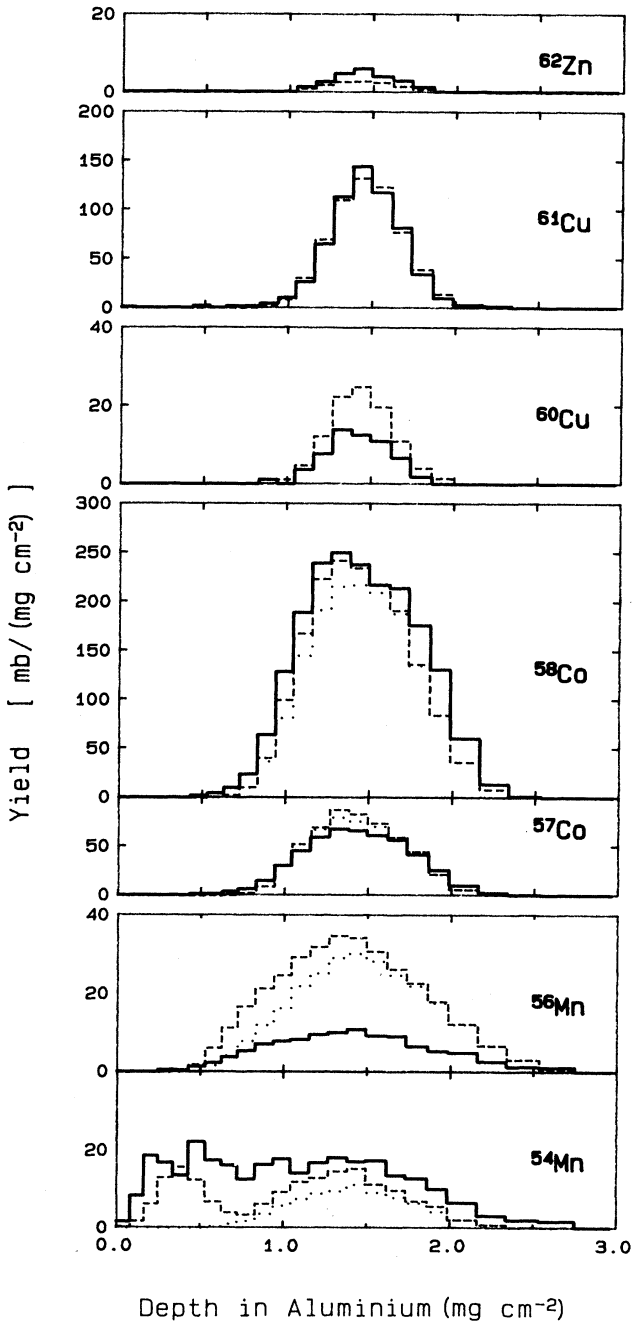

FIG. 3. Measured recoil range distributions of radioactive residues from reactions of 90 MeV ^{15}N on ^{51}V (solid histograms). The dotted histograms show the modelled distributions predicted on the basis of complete fusion alone; the dashed histograms show the modelled predictions for the various incomplete fusion modes in addition to complete fusion.

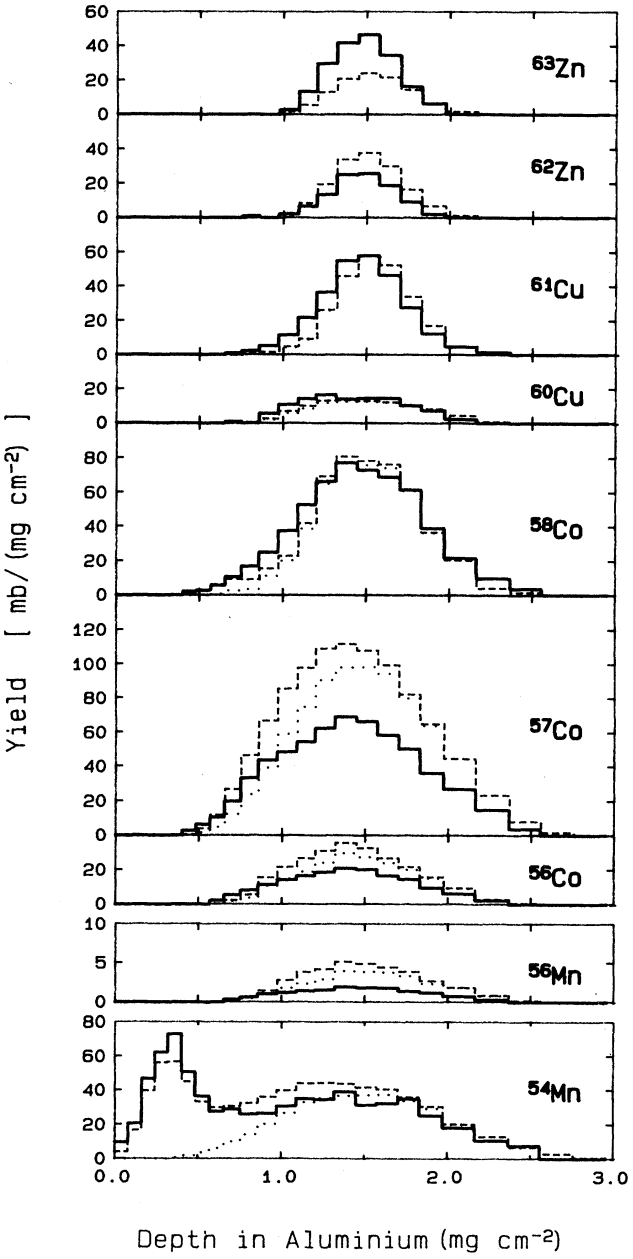

FIG. 4. As Fig. 3, for 96 MeV ^{16}O on ^{51}V.

The same effect is present to a small extent in the ^{54}Mn distribution obtained using the ^{20}Ne projectile.

III. INTERPRETATION OF RESULTS

A. Summary of the data

The data from these measurements are qualitatively similar to those obtained in our previous studies of fusion processes in $^{12}C+^{51}V$ (Ref. 3) and $^{20}Ne+^{93}Nb$ (Ref. 4) reactions, and a similar procedure has been followed in modelling and interpreting the data. Qualitatively, most

of the measured recoil distributions (Figs. 3–6) are apparently as expected for residues from complete fusion (a distribution symmetric about the depth to which the compound nucleus would recoil), but it is evident that processes other than complete fusion are involved in forming the residue ^{54}Mn in each case. From all four of the entrance channels, the recoil distribution for this product has a mean range much shorter than that for complete fusion; from three out of the four channels this distribution shows a pronounced peak at the range corresponding to fusion of a single α particle with the target.

In Sec. III B, the results expected for the yields and recoil distributions of the products on the basis of complete fusion alone will be calculated. Comparison with the data shows reasonable agreement except in the case of the product ^{54}Mn, for which complete fusion predicts much smaller yields than observed. However, there is also some indication of other processes contributing to formation of the products just above ^{54}Mn in mass.

The light-particle spectra of species with $Z > 2$ are characteristic of fragments from projectile breakup. They peak at an energy corresponding approximately to beam velocity, and their intensity falls off exponentially with angle. The spectra for fragments significantly lighter than the projectile are roughly symmetric about

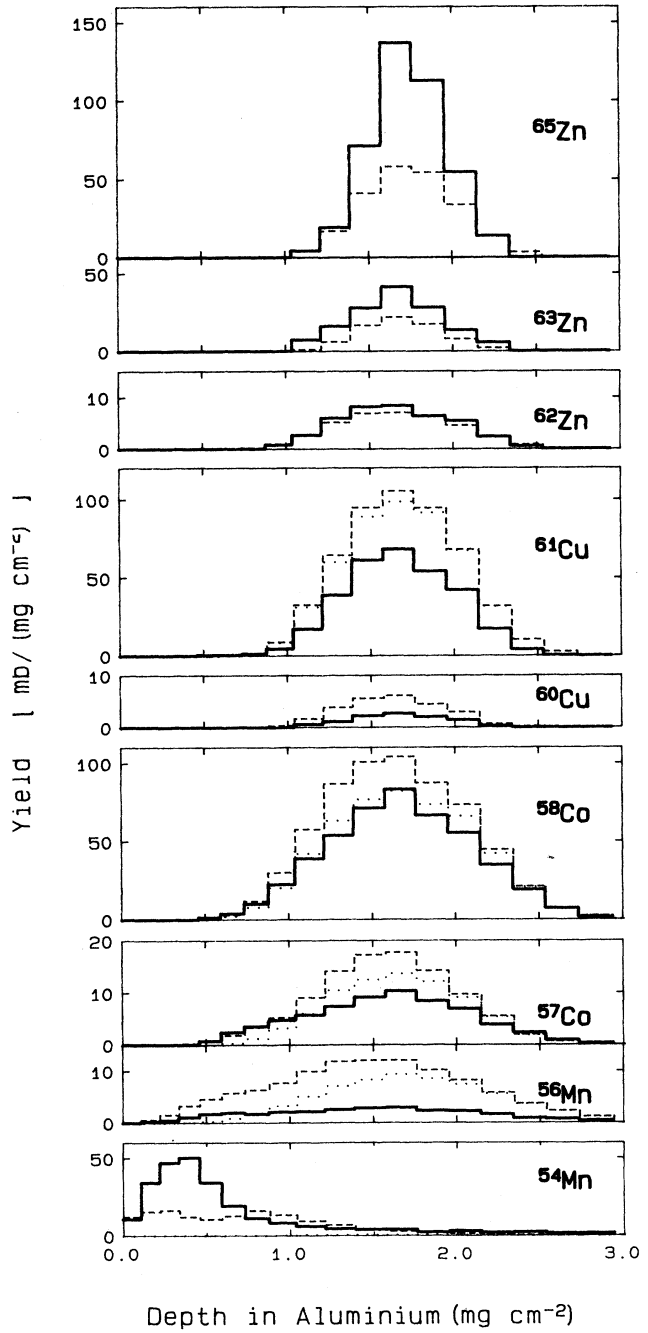

FIG. 5. As Fig. 3, for 115 MeV ^{19}F on ^{51}V.

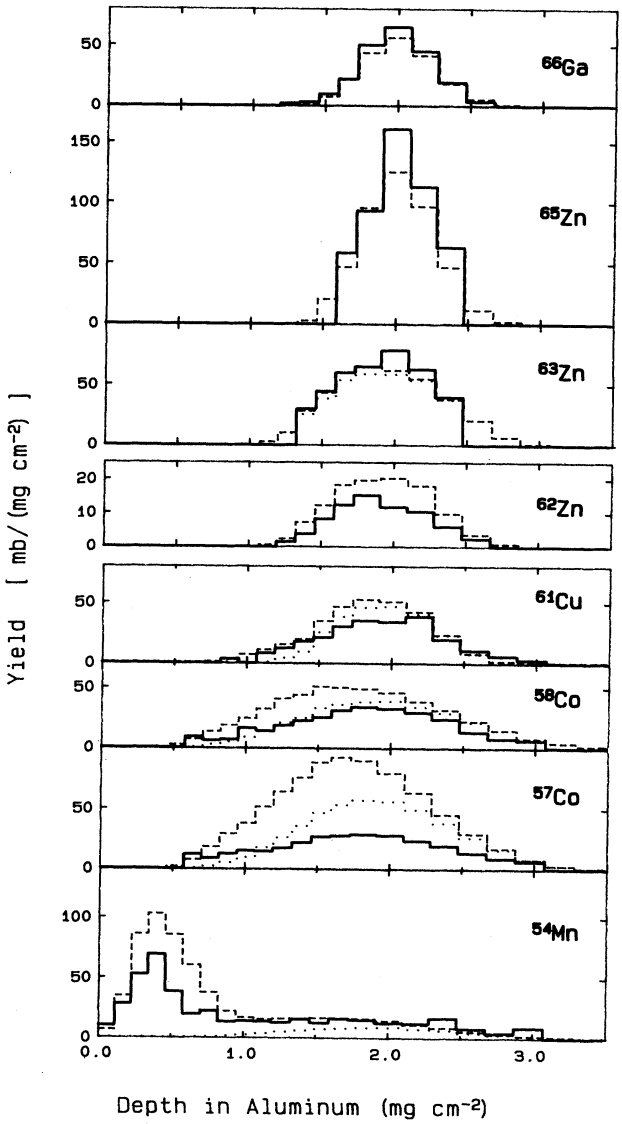

FIG. 6. As Fig. 3, for 120 MeV ^{20}Ne on ^{51}V.

the beam velocity, but those for fragments close to the projectile (e.g., the nitrogen spectra in Fig. 2) are distinctly asymmetric, and some include relatively sharp features.

The α-particle spectra are dominated by α's evaporated during the deexcitation process, and have the characteristic Maxwellian energy spectrum. In the centre-of-mass frame such evaporation spectra must be symmetric about 90°, but in the laboratory frame the yield is concentrated at forward angles (and the spectrum is displaced to higher energy at forward angles and to lower energy at backward angles). We have used the statistical-model code CASCADE (Ref. 5) to calculate the energy spectra of evaporated α particles expected from the reaction under consideration. Then we have parametrised their centre-of-mass angular distribution as

$$\frac{d^2\sigma}{dE_{\text{c.m.}}\, d\Omega_{\text{c.m.}}} = a + b\cos^2\phi + \frac{c}{\sin\phi}$$

and, transforming this distribution into the laboratory frame, have attempted to fit the parameters a,b,c to the measured spectra. It is found that satisfactory fits cannot be achieved, as the measured spectra are too intense at forward angles. Fitting to the backward-angle spectra alone results in the fits shown by the smooth curves in Fig. 1(a), and subtraction of these curves (which represent the true evaporative part of the spectra) from the measured spectra reveals the additional component shown in Fig. 1(b), which is again characteristic of fragments from projectile breakup. It should be noted that at higher incident energies this second component can be distinguished in the α-particle spectra without depending on the modelling process we have described; unfortunately at 6 MeV/nucleon the peak of the evaporation spectrum just happens to coincide with beam velocity.

The CASCADE calculations will be discussed further. Here it is pertinent to note that the intensity of the evaporative part of the measured α-particle spectra was in all cases within 10% of that predicted by CASCADE for complete fusion.

Thus, significant yields of projectile-like fragments of various species are observed, characteristic of fragments from projectile breakup. Integrating the energy spectrum at each angle, and extrapolating the resulting values for $d\sigma/d\Omega$ forward to 0°, one can obtain an estimate for the total yield of each type of fragment. The values obtained are listed in Table III; the uncertainty on each of these values is probably around 20%.

As in a previous paper,[4] we shall adopt the hypothesis that essentially all of these fragments are the spectator fragments from a binary process of incomplete fusion, in which the remainder of the projectile fuses completely with the target nucleus. Starting from this hypothesis, and a few other assumptions, we shall model the yields and the shapes of the recoil distributions which would be expected for the various product residues due to incomplete fusion as well as complete fusion, and compare these with our measured data. It transpires that the residues which we detected in this study, with the exception of ^{54}Mn, are not predicted to be strongly populated by incomplete fusion, so that the results of the modelling, including the incomplete fusion processes, are not dramatically different from those for complete fusion alone; nevertheless, the overall agreement with the data is certainly improved by incorporation of the incomplete fusion processes.

B. Modelling: Complete fusion

The residue yields expected from complete fusion for each of the four entrance channels were calculated using the code CASCADE (Ref. 5). As in our previous work[3,4] the fusion cross section for complete fusion was assumed to be equal to that bounded by the hard grazing partial wave l_g, calculated using the liquid drop potential formalism of Wilczynski and Siwek-Wilczynska.[9] This assumption gave reasonable results for ^{12}C+^{51}V and ^{20}Ne+^{93}Nb, although it conflicts with the results of other workers who find, for heavier systems, that this cross section encompasses the various incomplete fusion processes as well as complete fusion.

The parameters used in the CASCADE calculations were based on the work of Kicinska-Habior *et al.*,[10] who recently published an extensive study of γ-ray spectra from decay of the ^{63}Cu compound nucleus formed at excitation energies up to 77.4 MeV, in which they compared the success of CASCADE calculations using different parameter sets. They used an extended form of the CASCADE code, incorporating the giant dipole resonance and both the isoscalar and isovector giant quadrupole resonances; they found that in order to reproduce their data, they needed to reduce the level density parameter, a, at high excitation (the liquid drop region, above 20 MeV) from the standard value of $A/8$ MeV^{-1}. We find that we need the same reduction. The effect of the change is to enhance the importance of γ-ray emission as a deexcitation process; use of the standard level density in the present work leads to a serious underestimate of the

TABLE III. Total yields (in mb) of detected projectile-like fragments from the various projectiles [the result obtained using 72 MeV ^{12}C (Ref. 3) is included for comparison].

Projectile	^{12}C	^{15}N	^{16}O	^{19}F	^{20}Ne
α	480	200	180	320	420
B		20	13	12	
C		85	80	60	60
N			100	90	50
O				140	150

yields of the heaviest products, which can only be formed by complete fusion. Accordingly, we have used the same code as Kicinska-Habior *et al.* and have adopted their parameter set *F*, which best reproduced their data ($a = A/9.5$ MeV^{-1}, Δ calculated from Myers droplet masses without Wigner term, giant-resonance parameters all as in Ref. 10). However, these calculations appeared to overestimate the importance of α-particle evaporation; to improve agreement with our data we have additionally increased the value of the radius parameter used in calculating the liquid drop yrast line from the default value of 1.26 to 1.32 fm (it appears that Kicinska-Habior *et al.* would not have been particularly sensitive to the value of this parameter).

This parameter set has been used throughout the present work. Its use in the calculations for the $^{12}C+^{51}V$ channel, previously published,[3] improves still further the good agreement with the data. However, it should be noted that we have not attempted an extensive investigation of alternative parameter sets; it is possible that the agreement with the data could be somewhat improved by further adjustments to the parameters.

The CASCADE predictions for residue yields from complete fusion are listed in Table II for each of the four entrance channels. Comparison with the measured yields in the same table shows quite good agreement for all the products except ^{54}Mn, whose yield is underestimated in all cases (and in the case of the ^{19}F channel by almost 2 orders of magnitude) and ^{56}Mn, whose yield is overestimated by factors of 2 to 2.5. The measured yields of all the remaining products are within a factor of 2 of the CASCADE prediction for complete fusion except for the weak yield of ^{60}Cu from ^{19}F (1.9 mb instead of the predicted 4.9 mb), and for the most part are much closer than this. In general this would be considered good agreement for such statistical-model calculations, and is an indication that production of these residues is dominated by complete fusion, and that the parameters used in the code are appropriate. There is no indication that the CASCADE predictions are systematically either too high or too low, indicating that the fusion cross sections used are approximately correct (this is also supported by the good agreement found with the total yields of evaporated α particles, as mentioned in the preceding section).

The shapes of the recoil distributions expected for these residues, if produced by evaporation following complete fusion, were modelled, by a Monte Carlo approach, as described previously.[3,4] The modelling process starts with the compound nucleus recoiling with well-defined velocity along the beam axis and calculates the distribution of recoil velocity and angle of a residue formed by a

TABLE IV. Mean recoil ranges of radioactive residue from the four entrance channels (mg/cm^2 of aluminium).

				$^{15}N+^{51}V$					
	^{62}Zn	^{61}Cu	^{60}Cu	^{58}Co	^{57}Co	^{56}Mn	^{54}Mn		
Measured	1.44	1.45	1.41	1.43	1.42	1.36	1.00		
Modelled									
C.F.	1.43	1.46	1.44	1.44	1.42	1.45	1.40		
Total	1.43	1.46	1.44	1.43	1.42	1.36	1.03		
Without ^{8}Be	1.43	1.46	1.44	1.41	1.42	1.38	1.04		
				$^{16}O+^{51}V$					
	^{63}Zn	^{62}Zn	^{61}Cu	^{60}Cu	^{58}Co	^{57}Co	^{56}Co	^{56}Mn	^{54}Mn
Measured	1.47	1.46	1.46	1.40	1.43	1.37	1.36	1.42	0.90
Modelled									
C.F.	1.52	1.50	1.54	1.49	1.50	1.47	1.45	1.52	1.45
Totals	1.52	1.50	1.54	1.48	1.45	1.39	1.41	1.48	1.00
Without ^{8}Be	1.52	1.50	1.53	1.46	1.49	1.40	1.41	1.50	1.01
				$^{19}F+^{51}V$					
	^{65}Zn	^{63}Zn	^{62}Zn	^{61}Cu	^{60}Cu	^{58}Co	^{57}Co	^{56}Mn	^{54}Mn
Measured	1.73	1.66	1.65	1.67	1.66	1.65	1.55	1.39	0.59
Modelled									
C.F.	1.74	1.69	1.66	1.69	1.62	1.68	1.64	1.71	1.69
Totals	1.74	1.69	1.64	1.68	1.62	1.63	1.56	1.42	0.67
Without ^{8}Be	1.74	1.69	1.63	1.67	1.62	1.63	1.55	1.44	0.63
				$^{20}Ne+^{51}V$					
	^{66}Ga	^{65}Zn	^{63}Zn	^{62}Zn	^{61}Cu	^{58}Co	^{57}Co	^{54}Mn	
Measured	1.97	2.02	1.88	1.88	1.88	1.74	1.69	0.96	
Modelled									
C.F.	1.99	2.00	1.92	1.89	1.92	1.88	1.86	1.85	
Totals	1.99	2.00	1.90	1.89	1.80	1.70	1.67	0.78	
Without ^{8}Be	1.99	2.00	1.89	1.88	1.83	1.75	1.70	0.80	

specified sequence of particle evaporations, where the energy of each evaporated particle is given by the appropriate Maxwellian distribution and its angular distribution is either isotropic (for nucleon evaporation) or somewhat anisotropic (for α-particle evaporation); the final distribution of recoil velocities is then converted to a projected range distribution using a parametrisation of the range/energy tabulation of Northcliffe and Schilling.[11] These modelled distributions were then normalised to the yields predicted by CASCADE for complete fusion; the resulting modelled distributions are shown by the dotted histograms in Figs. 3–6. Again, with the exception of the results for ^{54}Mn, these appear to be in reasonable agreement with the measured range distributions, confirming that production of these residues is dominated by complete fusion.

The mean depths of the measured and modelled range distributions are listed in Table IV. Here it can be seen that, while the modelling reproduces the mean depth for the heavier residues in all cases to within 50 μg/cm^2 or 3% (within the experimental uncertainties), the modelled depths for the lightest residues are all greater than the corresponding measured values. This effect is of course most pronounced for the residue ^{54}Mn, but is also seen consistently for ^{56}Mn and, except from the lightest projectile ^{15}N, for ^{57}Co. This is an indication that processes such as incomplete fusion contribute, albeit to a small extent, to formation of these lighter residues.

C. Modelling: Incomplete fusion

Modelling of the incomplete fusion processes present is based upon the measured spectra of projectile-like fragments. If one assumes that incomplete fusion involves simple binary fragmentation of the projectile, in which one fragment (the "spectator") is emitted in its ground state while the other fuses completely with the target nucleus, then detecting the energy and angle of emission of the spectator enables one to deduce not only the velocity and angle of recoil of the fused intermediate but also its excitation energy (via the Q value for the reaction). Since the spectator fragment is emitted with a distribution of recoil energies and angles, the excited intermediate in each incomplete fusion process is populated with an extended distribution of recoil velocities, recoil angles, and excitation energies; this then provides the starting point for the second stage of the reaction mechanism, in which the excited intermediate decays by statistical evaporation. This decay process may be modelled using a statistical-model code. In this modelling it is also necessary to make some assumption concerning the angular momentum imparted to the intermediate, but this can be done with some confidence since there have now been several experimental studies of this point.[2]

The details of the modelling process were, with one exception, as described in Ref. 4, and are summarized very briefly here. At 6 MeV/nucleon, fusion of a fragment of mass m (u) was assumed to populate the fused intermediate with an angular momentum $2m\hbar$. For each possible fusion mode, CASCADE calculations were performed as a function of excitation energy with the value of the angular momentum fixed at this value; from these calculations one obtained the probabilities of populating the various residues from each intermediate as a function of excitation energy. The measured projectile-like fragment spectra were then parametrised using the empirical form

$$\frac{d^2\sigma}{dE\,d\Omega}=\sigma_0 \exp\left[\frac{-\theta}{\theta_0}\right]\left\{\exp\left[\frac{E-(E_0-k_1\theta-k_2\theta^2)}{\omega_1}\right]+\exp\left[\frac{E+(E_0-k_1\theta-k_2\theta^2)}{\omega_2}\right]\right\},$$

where the parameters E_0, k_1, k_2, θ_0, ω_1, ω_2, and σ_0 were determined by least-squares fitting to the data. Using a Monte Carlo approach, the corresponding distribution of excitation energies for the intermediate was calculated and weighted by the curves calculated using CASCADE, so as to give finally the expected yields of the various product residues from this incomplete fusion process.

In principle, given the assumptions just stated, and accepting that the parameters of the CASCADE calculation have already been adjusted so as to reproduce the complete fusion part of the yields, this prescription is all that is required to predict the absolute yields of the various residues from the various incomplete fusion processes.

However, two complications affect interpretation of the measured projectile-like fragment spectra. The first arises from the technical limitation that our data were unable to distinguish between different isotopes of heavy fragments so that we have to make some assumption as to which isotopes are emitted. For the purpose of all the modelling later discussed, we have made the assumption that all of the observed boron is ^{11}B, all of the observed carbon is ^{12}C, and all of the observed nitrogen is ^{15}N. Q-value arguments suggest that these are the isotopes most likely to be emitted; however, other isotopes (in particular ^{14}N) are almost certainly present, and will slightly distort the results obtained.

The second complication is more fundamental and concerns the possible presence of ^{8}Be as a projectile-like fragment. Any ^{8}Be emitted will break up into two α particles before detection, adding to the observed yield of α-particle fragments. The modelled yields will of course be somewhat different depending on whether we assume all the observed α-particle fragments to have been emitted originally as α's, or some significant proportion of them to be attributable to ^{8}Be emission. In our study of ^{12}C on ^{51}V, where it was possible to distinguish the contributions of the two incomplete fusion processes explicitly in the recoil distribution, it was found that, at 6 MeV/nucleon,

approximately half of the observed α-particle fragments in fact arose from ^{8}Be (since each ^{8}Be gives rise to two α particles, this means that the cross section for ^{8}Be emission was half that for α-particle emission). A similar ratio is predicted for all these entrance channels by the sum rule model of Wilczynski *et al.*,[12] which will be briefly discussed in Sec. III D. Accordingly, we have carried out our modelling under the assumption that half of the detected α particles are truly the original spectator fragments from incomplete fusion, while the other half are decay products arising from ^{8}Be spectators having twice the energy and half the yield. In the results which follow, we also present the corresponding values assuming no ^{8}Be emission at all.

For each of the various incomplete fusion processes corresponding to detected spectator fragments, the predicted contributions to the yields of the residues studied are listed in Table II, under the yields predicted from complete fusion. The total yield predicted from all these processes should be compared in each case with the measured yield. It can be seen that for the residue ^{54}Mn, whereas complete fusion alone was totally unable to account for the observed yields, the combination of complete fusion and the various modelled incomplete fusion processes reproduces the observed yield to within a factor of 2 for each of the four entrance channels. For some of the other residues, inclusion of the modelled incomplete fusion yields slightly worsens the agreement with the data; nevertheless, with the exception of production of ^{56}Mn, which is overestimated in all cases by a factor between 2.5 and 4, and production of ^{57}Co from ^{20}Ne (123 mb rather than the 44 mb observed), all of the modelled yields are still within a factor of 2 of the observed yield, which would generally be considered good agreement for such calculations.

Table II also lists the yields modelled ignoring the possibility of ^{8}Be emission and assuming that all the observed α-particle fragments should be treated as primary spectators. Overall, the agreement with the data is perhaps slightly worse in this case, but the difference is hardly significant.

More detailed evidence for the contributions of the incomplete fusion processes comes from modelling their contributions to the recoil distributions. The same Monte Carlo approach described in Sec. III B was used for this, but instead of taking the starting point as the compound nucleus recoiling with fixed velocity and excitation energy, each simulation started with the relevant incomplete fusion intermediate with the distribution of recoil velocities, angles, and excitation energies obtained from the distributions of the corresponding spectator, as previously described. An important point arises here. Ideally, the recoil distribution should be calculated in the course of the full statistical-model calculation of the decay of the intermediate, but this was not practicable and so, as described already, we calculated the recoil distribution separately and used CASCADE to predict the yield. For complete fusion, this separation is perfectly allowable, since all recoils start with the same velocity and excitation energy, but following incomplete fusion the recoil velocity and excitation intermediate is related to its excitation energy, which in turn affects what the final residue will be. Thus, from the same incomplete fusion process, different residues are formed predominantly from different parts of the initial distribution of the recoiling intermediate and will thus have different mean ranges (products requiring a large number of evaporation steps and hence a large initial excitation energy come on average from deeper in the range distribution). This effect is taken account of rather crudely in the present Monte Carlo calculations by keeping track at each stage of the excitation energy remaining (accounting for the binding energy and kinetic energy carried away by each evaporated particle) and only including in the construction of the final range distribution simulations which leave the final residue within a specified span of excitation energy. In previous studies[3,4] we have specified this to be the span 0–12 MeV (the evaporation sequence must be energetically possible and leave the final residue with less than 12 MeV of excitation energy). However, this takes no account of deexcitation by emission of γ rays, which we have already assumed to be an important process in these reactions. Instead, we specify the final excitation span for each residue as $E\gamma-8$ to $E\gamma+8$ MeV, where $E\gamma$, the mean energy carried away by γ-ray emission in formation of this particular product by this evaporation route, is obtained by comparing the excitation energy at which the CASCADE calculations for this process predict the yield of this residue to be at its maximum with the amount of energy typically absorbed by the evaporated particles' binding energies and kinetic energies.

The recoil distributions obtained by superimposing the modelled contributions of the various incomplete fusion processes on the modelled distributions from complete fusion are shown by the dashed histograms in Figs. 3–6. Their means are listed in Table IV.

The agreement with the measured means is satisfactory, and significantly better than that obtained assuming complete fusion alone. Only three cases (all involving production of ^{54}Mn) now disagree by more than 6%, and in most cases the agreement is much better than this. It is perhaps significant that the calculated values for the ^{16}O+^{51}V entrance channel are all higher than the data, by an amount ranging from 20 to 80 μg/cm^2 for the products heavier than ^{54}Mn (and by 100 μg/cm^2 in the case of ^{54}Mn); this may reflect a small systematic experimental effect in the data from this channel. From the remaining entrance channels, if we exclude production of ^{54}Mn, only one of the 21 calculated values differs from the observed value by more than 3% (the value for ^{61}Cu from ^{20}Ne is 4.5% lower than observed), which is impressive agreement.

The calculated values for the product ^{54}Mn agree much better with the observed values than those calculated excluding incomplete fusion, being within 100 μg/cm^2 of the observed values except for the ^{20}Ne channel; this last discrepancy is not significant since these data are known to be contaminated by ^{54}Mn produced by reactions on potassium in the catcher stack, which will artificially increase the measured mean range. In several cases the agreement is significantly worse, though still acceptable, if the possibility of ^{8}Be emission is ignored.

It should also be noted that in several cases the agreement with the shape of the measured recoil distribution would be significantly worsened if the effect of γ-ray emission, discussed above, were neglected. This apparently confirms that this emission is occurring.

It thus appears from consideration of the mean ranges that, even in those cases where incorporation of the incomplete fusion contributions made the discrepancy between the modelled and measured values for the total yield worse, incomplete fusion processes are involved at approximately the level assumed here, and that the discrepancy in modelling the total yields is attributable to shortcomings in the CASCADE calculations, which may overestimate or underestimate the contribution to formation of a specified residue by up to a factor of 2. Even in those cases where the total yield is incorrectly predicted, the shape of the recoil distribution is much better reproduced when the incomplete fusion processes are included than assuming complete fusion alone (as an example, see the case of production of ^{56}Mn from ^{19}F). The fact that yields of ^{56}Mn are consistently overestimated suggests that the level densities used for this nuclide may be erroneous.

However, it must be emphasised that incomplete fusion apparently makes a major contribution to formation of only one of the residues studied in this work, ^{54}Mn. The real test of our approach is thus how well it reproduces the observed recoil distributions for this nuclide. When we look at these in detail (Figs. 3–6) we find mixed success. That from ^{16}O is reproduced extremely well. For the other entrance channels, the detailed agreement is less good, but, loosely speaking, the modelled distributions can be said to agree with the measured distribution at each point to within approximately a factor of 2. Remembering that each modelled ^{54}Mn distribution is composed of between 4 and 6 superimposed distributions, each normalised using a CASCADE calculation whose result may be in error by up to a factor of 2, the agreement with the data must be regarded as reasonable.

Summarising these results, within the limitations of the statistical-model calculations, modelling based on the hypothesis that all of the observed projectile-like fragments are spectator fragments accompanying incomplete fusion does consistently reproduce the data, and significantly better than modelling of complete fusion alone. However, the data are not sufficiently sensitive or complete to enable us to conclude whether this hypothesis (for which there was stronger evidence in earlier studies) is actually true in detail.

D. The sum-rule model of incomplete fusion

In 1980 Wilczynski *et al.*[12] proposed a simple semi-empirical sum-rule model which has apparently had considerable success in predicting the total cross sections for the different possible incomplete fusion modes for a given projectile/target entrance channel. This is based on a picture in which for each possible fusion mode fusion becomes unfavourable when the angular momentum of the fusing particle becomes so large that the net potential at the point of contact with the target is no longer attractive. In incomplete fusion the angular momentum of the incident projectile is shared between the two fragments roughly in proportion to their masses; for a given bombarding energy, as the incident angular momentum is increased, fusion of heavier fragments will become impossible and fusion of lighter fragments will take over. This overall picture is now generally accepted. The sum-rule model further supposed that all of these fusion processes extend in l space up to the hard grazing partial wave, l_g, calculated using some simple potential, and that above l_g no fusion takes place. Below l_g, competition between the possible fusion modes is also influenced by their respective ground-state Q values, to an extent depending on an empirical temperature parameter.

Following our assumption that the yields of fragments listed in Table III are in fact the total cross sections for the corresponding incomplete fusion modes, we have attempted to reproduce these using the sum-rule model. However, taking the value of l_g from the liquid drop potential of Wilczynski[13] using point-charge Coulomb potentials, as recommended by Wilczynski *et al.*,[12] anomalously small values were predicted for the complete fusion cross section and essentially no incomplete fusion at these energies. Use of Wilczynski and Siwek-Wilczynska's more realistic Coulomb potential inside the nucleus[9] gave larger fusion cross sections, but still very little incomplete fusion (these were the values used for the fusion cross section for complete fusion in the CASCADE calculations reported above). In order to get the model to predict significant yields for incomplete fusion, it was necessary to increase the value of l_g by a further 10%. Then use of the original sum-rule parameters of Wilczynski *et al.*[12] ($T=3$ MeV, $\Delta=2$, $R_c=2$ fm) showed some prospect of agreement with our data. Reducing Δ to 1.5 gave quite reasonable agreement with the cross sections listed in Table III—in all cases the predicted yields were within a factor of 2 of our observed yields.

If, therefore, we accept that our data do indicate that incomplete fusion processes are present at something approaching these levels, we must conclude, within the framework of the sum-rule model, that the various fusion processes extend to partial waves significantly higher than the conventional hard grazing wave. We have previously reported the same conclusion in studies of ^{12}C on ^{51}V and ^{20}Ne on ^{93}Nb, and this would suggest that the sum-rule picture, which was developed for somewhat heavier systems, may need to be modified in this regard when applied to medium mass systems. If one extends the span of partial waves included by this means, it is probably still possible to account for the observed cross sections within the remainder of the sum-rule formalism.

IV. CONCLUSIONS

The inclusive light particle spectra measured from the reactions of 6 MeV/nucleon ^{12}C, ^{16}O, ^{20}Ne, ^{15}N, and ^{19}F with a ^{51}V target show significant yields of various species characteristic of fragments arising from projectile breakup, emitted at forward angles with velocities close to the beam velocity. One possible explanation for these fragments is that they are the spectator fragments associated

with various incomplete fusion processes, though conventional models of incomplete fusion would not predict this to be very important for these systems at such a low energy.

In order to investigate the importance of incomplete fusion in these reactions we have measured residue cross sections and recoil range distributions for a number of radioactive product residues, and compared these with the predictions of a statistical-model calculation of complete fusion. These calculations reproduce the residue yields and recoil distributions for all the heavier residues fairly well, but notably fail to account for the production of the residue ^{54}Mn. It is clear that incomplete fusion processes, and in particular the process in which a single α particle fuses with the target, are largely responsible for formation of this product. This result is somewhat at variance with the predictions of the sum-rule model of incomplete fusion,[12] which supposes that fusion of a single α particle will only become important for partial waves above those involved in other incomplete fusion processes, and therefore that this fusion mode will only appear at significantly higher incident energies.

We have investigated the possibility that essentially all of the observed projectile breakup fragments are indeed spectator fragments associated with incomplete fusion, by calculating the yields and recoil distributions expected on this basis for the various observed residues. The results are consistent with all of the measured data—essentially all of the residue yields are reproduced to within a factor 2, and the mean ranges to within 5%; the shapes of the recoil distribution are also well reproduced. The data are thus consistent with the hypothesis that all of the observed projectile-like fragments arise from incomplete fusion, though the present data do not provide a very strong test of this hypothesis, as the residues studied, with the exception of ^{54}Mn, do not include those which are predicted to be most influenced by incomplete fusion processes. Much stronger evidence in favour of this hypothesis was found at similar incident energies in our earlier studies of ^{12}C+^{51}V (Ref. 3) and ^{20}Ne+^{93}Nb (Ref. 4).

It is therefore suggested that the measured fragment yields listed in Table III represent the cross sections for the various incomplete fusion processes in these reactions. Certainly the cross sections for the process in which a single α particle fuses with the target are approximately as implied by the yields of (projectile-α) fragments. We have briefly investigated how the sum-rule model[12] would have to be modified to reproduce these incomplete fusion cross sections; it appears that quite good agreement can be achieved, if the range of partial waves contributing to fusionlike processes is increased by approximately 10% over that assumed in the original formulation of the sum rule model. This corresponds to an extension of the model rather than a change to its philosophy, and may reflect the fact that the systems studied in the present work are somewhat lighter than those for which the model was developed. It is interesting to note that the sum-rule description almost inevitably implies that if the single α-particle fusion process is occurring at the observed levels, then other incomplete fusion processes must be present at approximately the levels implied by the yields in Table III.

ACKNOWLEDGMENTS

The authors are grateful for stimulating comments by Professor E. Gadioli, Dr. T. W. Conlon, and Dr. P. E. Hodgson, and for the assistance of Mr. S. Sugden in measuring the particle spectra. Mrs. M. Miller continues to prepare the necessary foils with great skill. J.J.H. was supported in this work by the Natural Sciences and Engineering Research Council of Canada. The work described in this paper was undertaken as part of the Underlying Research Programme of the United Kingdom Atomic Energy Authority.

[1]T. Inamura, M. Ishihara, T. Fukuda, T. Shimado, and H. Hiruta, Phys. Lett. **68B**, 51 (1977).

[2]See reviews by C. Gershel, Nucl. Phys. **A387**, 297c (1982); and R. H. Siemssen, *ibid.* **A400**, 245c (1983).

[3]D. J. Parker, J. Asher, T. W. Conlon, and I. Naqib, Phys. Rev. C **30**, 143 (1984).

[4]D. J. Parker, J. J. Hogan, and J. Asher, Phys. Rev. C **35**, 161 (1987).

[5]F. Pühlhofer, Nucl. Phys. A **280**, 267 (1977)

[6]J. A. B. Goodall, United Kingdom Atomic Energy Authority Report AERE-M3185 (1982).

[7]U. Reus, W. Westmeier, and I. Warnecke, At. Data Nucl. Data Tables **29**, 1 (1983).

[8]J. Wing and J. R. Huizenga, Phys. Rev. **128**, 280 (1962).

[9]J. Wilczynski and K. Siwek-Wilczynska, Phys. Lett. **55B**, 270 (1975).

[10]M. Kicinska-Habior, K. A. Snover, C. A. Gosset, J. A. Behr, G. Feldman, H. K. Glatzel, J. H. Gundlach, and E. F. Garman, Phys. Rev. C **36**, 612 (1987).

[11]L. C. Northcliffe and R. F. Schilling, Nucl. Data Tables **A7**, 233 (1970).

[12]J. Wilczynski, K. Siwek-Wilczynska, J. van Driel, S. Gonggrijp, D. C. J. M. Hageman, R. V. F. Janssens, J. Lukasiak, and R. H. Siemssen, Phys. Rev. Lett. **45**, 606 (1980).

[13]J. Wilczynski, Nucl. Phys. **A216**, 386 (1973).